Indian Journal of Pure & Applied Physics
Vol. 64, March 2026, pp. 292-303
DOI: 10.56042/ijpap.v64i3.25478

Studies on Semi-Organic Single Crystal of L-Histidinium Phosphite (LHPI) for Optical, Thermal, Mechanical and NLO Applications

Indu[a], Mahak Vij[b], Meenakshi[a] & Sonia[a*]

[a]Department of Physics, Baba Mastnath University, Asthal Boh ar, Rohtak, Haryana 124 021, India

[b]CSIR-National Physical Laboratory, New Delhi 110 012, India

Received: 14th November 2025; accepted:19th January 2026

A semi-organic nonlinear optical material L- histidinium phosphite (LHPI) was grown as a single crystal using an economic slow evaporation solution growth technique. To determine the structural information i.e., the unit cell parameters, Single Crystal XRD analysis was performed and found that the compound has a monoclinic crystal System with $P2_1$ non-centrosymmetric space group. Hirshfeld (HF) analysis and a 2-D fingerprint plot have been used to study the intermolecular interaction of the compound. Photoluminescence analysis revealed that the compound has green fluorescence emission. The specific heat of compound was calculated through Differential Scanning Calorimetry (DSC). The Laser damage threshold (LDT) of LHPI is 1.13 and 0.78 GW cm^{-2} for one and 10 pulse/second respectively. The frequency conversion property of this compound was studied through the Kurtz- Perry powder technique (SHG) and Z-Scan technique. Microhardness studies revealed that LHPI is a hard material. Through Shock Damage Threshold (SDT), the stability of the material against shock wave was assessed, which indicates that no damage appears up to the 5th shock.

Keywords: Crystal growth, Structural analysis, Differential scanning calorimetry, Nonlinear studies, Mechanical analysis

1 Introduction

Amino acid-based single crystals fascinate the consistent attention of the young researcher. As these materials exhibit high nonlinear efficiency due to the formation of zwitterions and most of these materials crystallize in non-centrosymmetric space groups[1,2]. The crystal hardness is the result of the molecule's zwitter-ionic activity. Among all the amino acids, L-histidine contains an imidazole group. This helps the L-histidine to show a good non-linear behaviour[2,3]. Non-linear optical materials are now a crucial component of many applications, including frequency generation, ultra-fast switches, laser amplifiers, photonics, optical data processing, and others[4,5]. Because of the growing need for such types of materials, researchers are increasingly focused on finding novel NLO materials that meet current needs. Based on the properties of materials, we can classify the NLO materials into three categories[6]. Inorganic materials are hard materials but they show less nonlinear behavior. Whereas, organic materials possess contrasting characteristics (high nonlinear response but have low sustenance against load and temperature[7]. According to the demands of various industries, the properties of organic NLO materials can be modified with the use of chemical engineering techniques[8]. A new category of NLO materials known as semi-organic has been established by improving the features of organic materials. These materials exhibit significant nonlinearity in addition to outstanding mechanical and thermal stability[9].

L-histidine is one of the amino acids that provide fascinating semi-organic non-linear optically active single crystals. Plethora of phosphite single crystals has been investigated with different amino acids such as- Glycine phosphite, L-Arginine phosphite, L-Prolinium phosphite etc[10-12]. In the present work, interaction of phosphorous acid with L-histidine amino acid was studied. Primarily L-histidine phosphite single crystal was reported by Madden et al. in 1972 in the orthorhombic system. This structure has low accuracy because it was a twinned structure and hydrogen atoms were not positioned accurately[13]. This twinned structure was reinvestigated by M.T. Averbuch- Pouchot et al. in 1993[14]. That study investigates the more accurate monoclinic structure of L-histidine phosphite with the $P2_1$ space group. Later on, various properties of L-histidine phosphite single crystals were investigated and reported by S. Shanmuga Sundari et al. in 2021[15]. This study

*Corresponding author: E-mail: ahlawat.sonia44@gmail.com

revealed that the titled compound was a ferroelectric crystal and can be used for sensors and optoelectronic applications. UV spectrum analysis showed that it was transparent material. The thermal properties of the sample were examined. Theoretical study of density functional theory proved that at room temperature LHPI expresses good NLO behaviour. Raman spectroscopy explained the stretching vibrations of different atoms in a compound i.e., stretching vibrations for N=H (3119 cm^{-1}), P=H (2406 cm^{-1}), C=O (1628 cm^{-1}) C=OH (1260 cm^{-1}), C=C (902 cm^{-1}), and COOH (452 cm^{-1}) were found. The FTIR spectrum of this compound was observed within the range of 4000-400 cm^{-1} for studying the bending and stretching of the functional group of the compound. An optical study revealed that LHPI was transparent in this region. The transition of the material from ferroelectric to paraelectric takes place at 270 ºC[15].

In the present work, the L-histidine phosphite (LHPI) single crystal was synthesized and subjected to various characterizations like: - XRD; HF analysis; NMR/ HETCOR; Photoluminescence; DSC; LDT; SHG; Z-Scan; Microhardness; SDT etc, to check its usage for various NLO application.

2 Experimental Section- Synthesis

L-histidine phosphite (LHPI) single crystals were synthesized using L-histidine and phosphorous acid purchasing from CDH as an initial reagent in equimolar ratio. In order to grow the LHPI single crystal, a saturated solution of the desired salts was prepared in distilled water with the help of a magnetic stirrer. Prepared saturated solution still contains some of the undissolved impurities which were removed by filtering the solution through Whatman filter paper. After that, a perforated sheet was placed over the solution, which was then left at room temperature to evaporate gradually. From the solution, single crystals of LHPI were obtained after 15-20 days. To ascertain the behaviour of the material, various characterizations to these crystals were applied. The structural conformation of the grown crystal was examined using XRD. Single crystal XRD confirms that the grown crystal was in good agreement with reported data[15].

3 Results and Discussion

In order to determine the behaviour of LHPI single crystal, the titled compound was subjected to various characterization techniques such as Single crystal-XRD, Hirshfeld surface analysis, Nuclear Magnetic Spectroscopy (NMR)/HETCOR, photoluminescence, DSC, second harmonic generation (SHG), LDT, SDT, Z-Scan, Vicker's hardness etc. for frequency conversion application.

3.1 SCXRD Analysis

To verify the crystal structure of the grown sample, an appropriate crystal was chosen, and Supernova, Single source at offset/far, HyPix3000 diffractometer was used to measure its structure. During data collection, the crystal was maintained at 293 K. In the SHELXT structure solution program using intrinsic phasing, the structure of the compound was solved using Olex2. In the SHELXT refinement package, the structure was refined using Least Square minimization[16-18]. According to the SCXRD investigation, it is found that LHPI crystallizes in a monoclinic crystal system with the non-centrosymmetric space group $P2_1$. The lattice parameters of the crystal were 4.9723(3) Å × 12.0101(6) Å × 8.5189(7) Å. Crystal data and structure refinement data of the titled compound was given by Table 1 and the grown crystal was represented by Fig. 1.

Table 1 — Crystal data and structure refinement

Compound Name	L-histidinium phosphite
Crystal System	monoclinic
Space group	$P2_1$
a/Å	4.9723(3)
b/Å	12.0101(6)
c/Å	8.5189(7)
α/º	90
β/º	104.160(7)
γ/º	90
Volume/ $Å^3$	493.27(6)
Z	2
ρ_{calc} (g cm^{-3})	1.590
μ/mm^{-1}	0.287
F (000)	246.0
Radiation	MoKα (λ= 0.71073)
2θ min/º	6.786
2θ max/º	46.428
Index ranges	$-4 \le h \le 5$, $-13 \le k \le 13$, $-9 \le l \le 7$
Reflections collected	1198
Independent reflections	815 [R_{int} = 0.0292, R_{sigma} = 0.0567]
Data/restraints/parameters	815/1/138
Goodness-of-fit on F^2	1.045
Final R indexes [$I \ge 2\sigma$ (I)]	R_1 = 0.0411, wR_2 = 0.1012
Final R indexes [all data]	R_1 = 0.0433, wR_2 = 0.1040
Largest diff. peak/hole/ e $Å^{-3}$	0.35/-0.23
Flack parameter	-0.12(19)

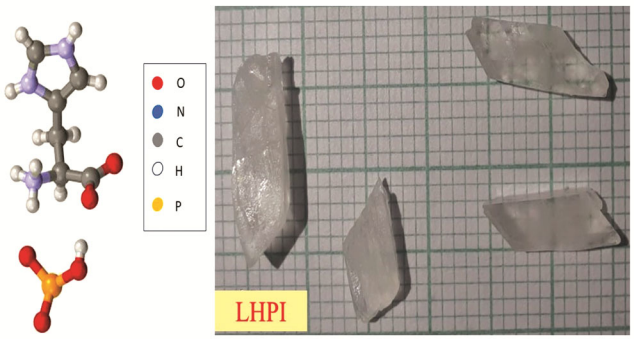

Fig. 1 — Crystal structure and grown single crystals of LHPI

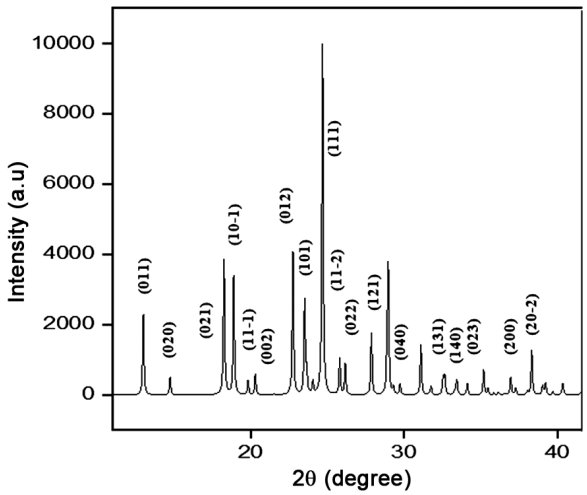

Fig. 2 — X-ray diffraction curve of LHPI

3.2 XRD Curve

For determining the phase correlation of the sample molecule, a powdered sample of the grown crystal was taken by crushing it with the help of agate mortar and pestle. The sample compound was placed under a powder X-ray diffractometer with MoKα radiation. The scanning range of 2θ for the sample was 10º - 70º with a scanning rate of 0.02º. The high-intensity sharp peaks were detected in the spectra which confirm that the grown crystal has excellent crystalline character. The observed peaks are found to be in good agreement with the reported data. The Powder X-ray diffraction curve of the titled compound is given in Fig. 2.

3.3 Hirshfeld Surface Analysis

An effective tool for the graphical representation of intermolecular interactions existing in the crystal lattice is the Hirshfeld surface (HF) analysis[19]. This surface is produced by the partition space in the crystal system using the contour of electron density. The weight of molecule density is taken into account while distributing the molecular density[20]. Every HF surface point contains two contact distances i.e., d_i and d_e. In this case, d_i stands for the contact distance between a point and an atom that is nearby inside the HF surface. On the other hand, the contact distance between that specific spot and the neighbouring atom, as being outside the HF surface was expressed by d_e[21]. By using the concept of normalized contact distance d_{norm}, it was possible to account for the interaction of atoms that were close to the surface from both inside and the outside[22]. The study of HF surfaces employs colour-coded data to identify the type of intermolecular interaction found in the crystal structure[23]. In the d_{norm} surface, there are mainly three coloured regions which easily explain the strength of interaction. These regions are red, blue, and white. Here, the red region signifies the strongest interaction whereas the blue region represents the overall weakest interaction, and the white region of the surface shows the weak interaction between the molecules[24].

Shape index and curvedness surface are the measures of surface as the principal curvature. In the shape index surface interaction is in the form of red and blue triangles, where blue triangles are in bump (convex) form and are because of carbon in the ring present inside the surface whereas the red region is in depression. Curvedness surface has two main regions where the flat green region is the major part which is separated by positive curvature i.e., blue edges[22-25]. Different colours of the fragment patch surface represent the interaction of external atoms to the nearest molecule[26,27]. These different surfaces of LHPI are represented in Fig. 3.

3.3.1 Fingerprint Plots

To analyze the intermolecular interaction of all the atoms at the same time or the different atoms separately, 2D fingerprint plots of HF surfaces were carried out using crystal explorer software[28,29]. Fingerprint plots corresponding to the interaction between different atoms were recorded for both the motifs (L-histidine and phosphite) of L-histidinium phosphite compound and represented in Figs. 4 and 5, respectively and the percentage interaction is represented in Table 2.

3.3.2 L histidine motif

The important connection was among H, O, C, N and other atoms. The long, narrow peak in the fingerprint pattern indicated the strongest contact. Some of the highest interactions are shown in Fig. 4.

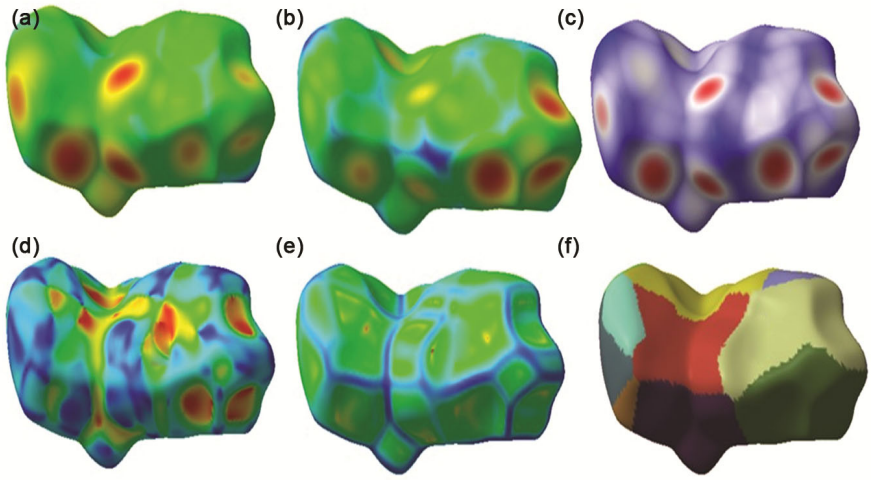

Fig. 3 — Hirshfeld surface of LHPI crystal with d_i, d_e, d_{norm}, shape index, curvedness, and fragment patch respectively

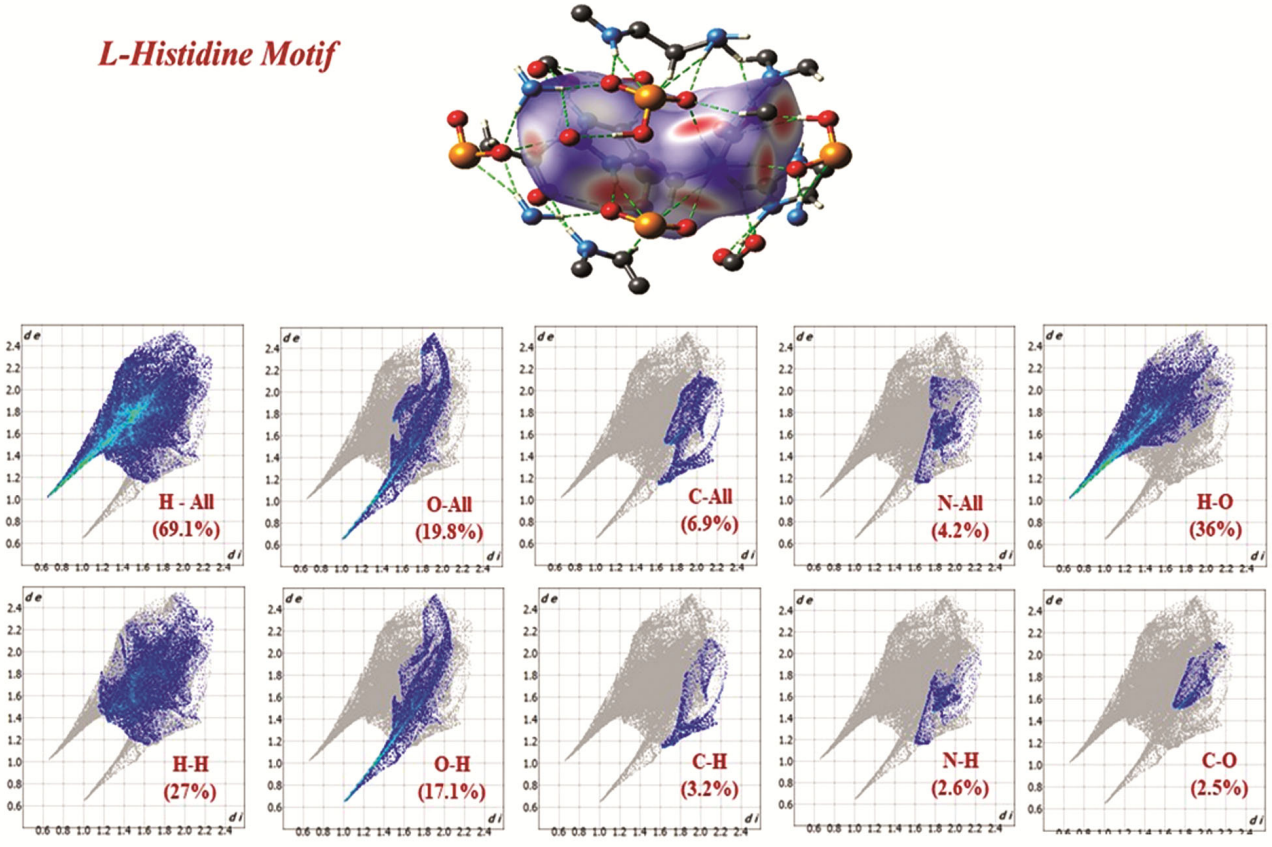

Fig. 4 — HF surface and 2D plot of L-Histidine Motif

In this motif, most of the interaction were resulting from H---All which was 69.1 %. The interactions of Hydrogen atoms with other atoms were as H---O (36 %), H---H (27 %), H---P (1.8 %), H---N (1.7 %) and H---C (2.7 %). After H-atom the strong interactions were formed by O-atom out of which the strongest contact was with H-atom i.e., O---H (17.1 %). Other significant interactions were C---H (3.2 %), N---H (2.6 %) and C---O (2.5 %).

3.3.3 Phosphite motif

The percentage contribution of interactions shown by atoms of phosphite motif of L-histidine phosphite was represented by Fig. 5. After the

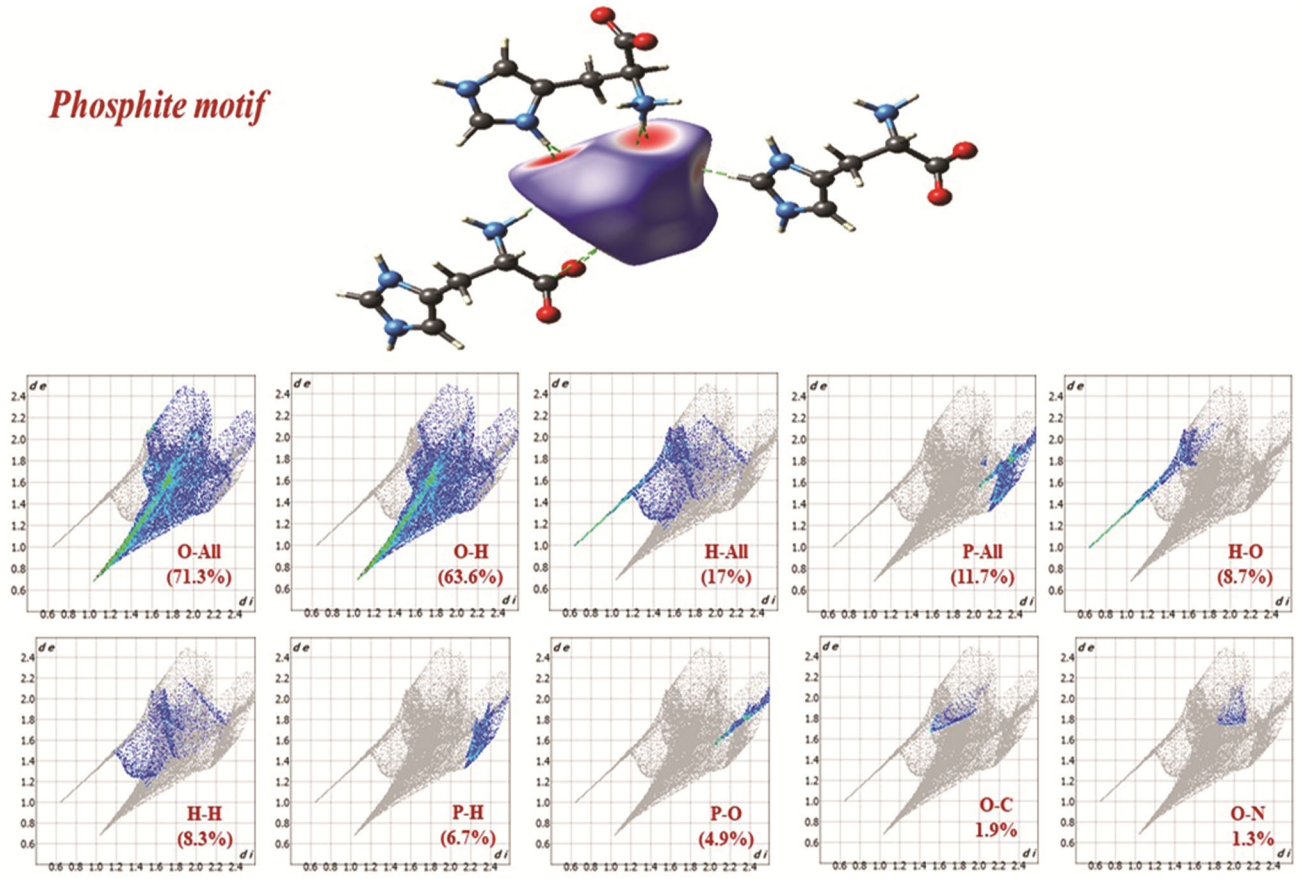

Fig. 5 — HF surface and 2D fingerprint plot of Phosphite motif

Table 2 — Interaction percentage b/w the atom of LHPI material in different motifs

L- histidine motif		Phosphite motif	
Interacting Atoms	Percentile Interaction	Interacting Atoms	Percentile Interaction
H-All	69.1	O-All	71.3
O- All	19.8	H-All	17
C-All	6.9	P-All	11.7
N-All	4.2	O-H	63.6
H-O	36	H-O	8.7
H-H	27	H-H	8.3
O-H	17.1	P-H	6.7
C-H	3.2	P-O	4.9
N-H	2.6	O-C	1.9
C-O	2.5	O-N	1.3

detailed analysis of 2D fingerprint plots of this motif, it was found that the strongest interaction was due to oxygen atoms as- O---All (71.3 %). In this plot, the contribution of O---H was (63.6 %) and for H---All was (17 %). Other significant contacts of atoms with one another were as-

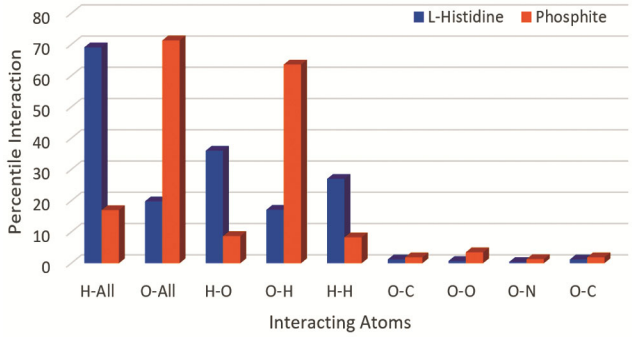

Fig. 6 — Comparative study of intermolecular interaction of different motifs of LHPI molecule

H---O (8.7 %), H---H (8.3 %), P---H (6.7 %), P---O (4.9 %).

The tabular form of percentage interaction between the different atoms of L-histidine and phosphite motifs of LHPI molecule is given below and the comparative study of intermolecular interaction of these motifs of LHPI molecule is represented by Fig. 6.

Fingerprint plots represent the interaction of atoms with other atoms in the molecule. In the histidine

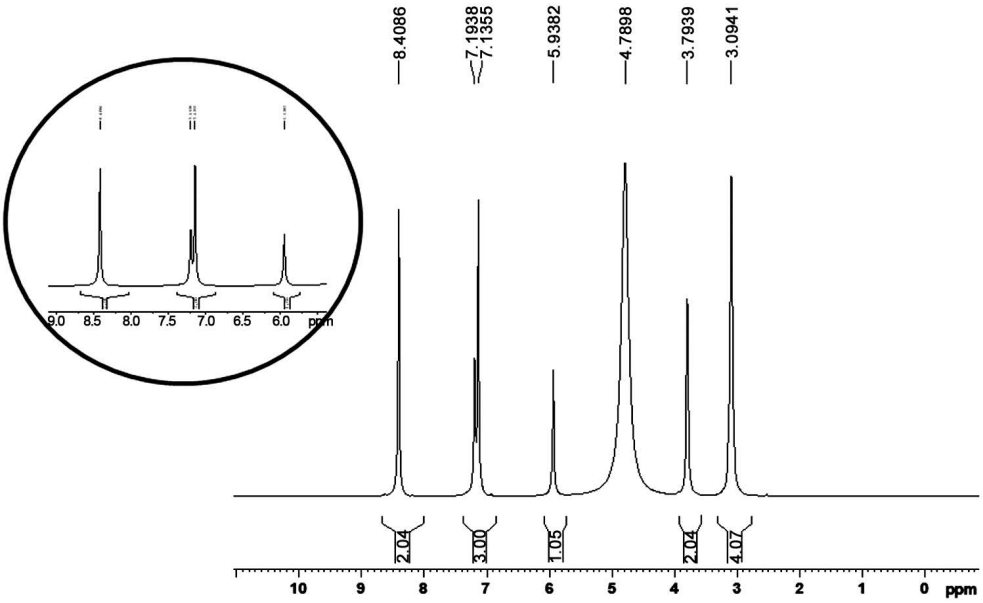

Fig. 7 — ^{1}H NMR spectra of LHPI

motif highest interaction is shown by the Hydrogen atom which is 69.1 % and least interaction shown by Nitrogen atom which is 4.1 %. In phosphite motif oxygen atom shows highest interaction (71.3 %) but the phosphorous atom shows least interaction i.e. 11.7 % in all.

3.4 NMR/HETCOR Analysis

The structural analysis of the titled compound was studied through NMR spectroscopy. The ^{1}H and ^{13}C NMR spectroscopy seems better for this purpose. This investigation was carried out by using BRUKER AVANCE NEO 500 MHz NMR spectrometer for ^{1}H at 300 K temperature with high resolution and C13CDP for 125 MHz at 300 K. The powdered form of the titled compound was dissolved in D_2O solvent and subjected to the spectrometer for NMR spectroscopy.

The observed peaks corresponding to the chemical shifts appear in the ^{1}H and ^{13}C NMR spectra are represented in Figs. 7 and 8, respectively. HETCOR analysis was represented by Fig. 9, which expressed hydrogen carbon correlation and revealed, which H-atom is bonded with which carbon atom.

In ^{1}H NMR, there are five singlets and one doublet. The singlet appeared at signal δ = 3.0941 ppm, 3.7939 ppm, 4.7898 ppm, 5.9382 ppm and 8.4086 ppm and the doublet was observed at 7.1355 ppm and 7.1938 ppm. The singlet corresponds to that single H- atom which had different environment around it and the doublet shows that two

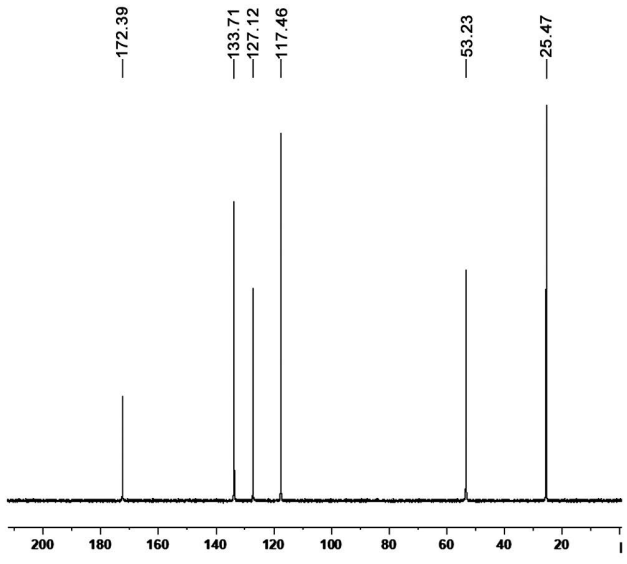

Fig. 8 — ^{13}C NMR spectra of LHPI

of the H-atom in the compound had the same environment in the structure.

The Chemical shift produced due to the carbon atoms was determined through ^{13}C NMR. On comparing the signal values with the structure (shown in Fig. 8), we observed that in C13CDP NMR, the signal at δ = 172.39 stands for the carbon in the acid. The δ values 133.71 ppm and 127.12 ppm are attributed to aromatic ring carbons. The shift value of 117.46 ppm was due to the carbon in alkene group. Carbon in the CH_2 group had a peak at 25.47 ppm.

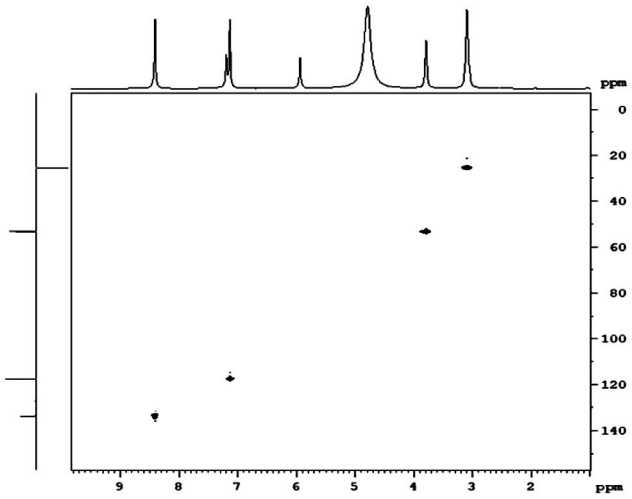

Fig. 9 — HETCOR spectra

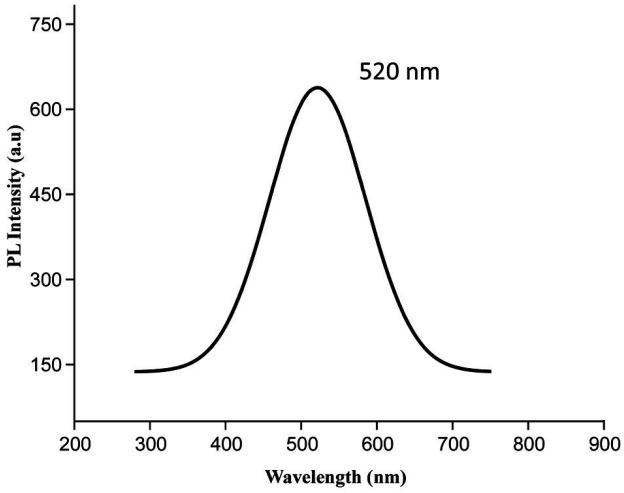

Fig. 10 — Photoluminescence curve

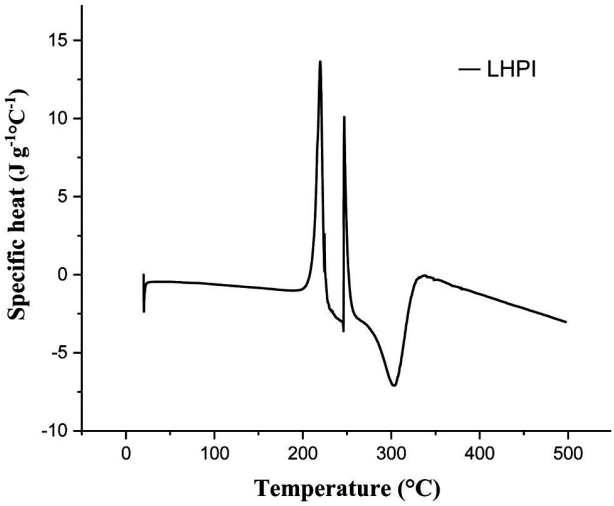

Fig. 11 — DSC curve for specific heat

3.5 Photoluminescence (PL) Spectroscopy

Out of **various** electromagnetic spectroscopy, Photoluminescence spectroscopy is the one that examines the fluorescence of the sample[30,31]. The instrument used for this purpose was a Spectrofluorophotometer (Model: RF-5301PC). The system used a xenon flash lamp as a source which gives highly intense light, this light was passed through the excitation monochromator followed by a polarizer filter that illuminates the sample with polarized light. Then the light emitted by the sample molecules was passed through the analyzer followed by an emission monochromator which passed the light to the photomultiplier tube where the fluorescence intensity was measured. Corresponding variation in the PL intensity with wavelength was measured and plotted using origin software. Data was collected within the wavelength range of 200 – 900 nm. The curve represented in Fig. 10 shows that this material was excited at 270 nm and the emission peak appears at 520 nm which corresponds to green light emission.

3.6 Differential Scanning Calorimetry (DSC)

Differential scanning calorimetry (DSC) studies are used for calculating the specific heat of LHPI material. The compound sample was exposed to the Perkin Elmer Pyris 6DSC instrument in a nitrogen environment with a flow rate of 20 ml min^{-1}. Under the temperature range 20 °C to 500 °C. The recorded data was then plotted through Origin software, which gives the curve of specific heat vs temperature as shown in Fig. 11. Highly intense peaks in the curve explain the perfect crystallites and the fine thermal stability of the crystal confirming the compound's suitability for non-linear applications[32]. From the data we obtained, the specific heat was calculated using the relation given below[33],

$$\Delta H = Cp.\ \Delta T \quad \ldots (1)$$

Here, C_p represents specific heat, ΔH= heat energy per unit mass. From curve analysis we find that maximum value of specific heat for LHPI is comes out to be 13.66 J $g^{-1}°C^{-1}$.

3.7 Laser Damage Threshold

The ability of a material to withstand against highly intense laser was measured by the LDT value of the material[34]. It was an important approach to determine the feasibility of material for nonlinear optics and laser application because it provides the limits to its

performance in various applications. The LDT value basically depends upon the laser beam i.e., beam size, wavelength, and energy, duration of the pulse, and especially the crystal's quality. A good quality crystal may have a high value of LDT which reflects the laser and mechanical stability of the material that makes it efficient for NLO application[35,36]. Through the Laser Damage threshold, we can also determine the mechanical strength of the sample. However, there are several inherent and extrinsic reasons which explains why the materials could experience laser-induced damage[37].

The optical strength of materials was decreased by intrinsic damage, which includes linear absorption, a few nonlinear processes including self-focusing, multi-photon absorption or two-photon absorption, stimulated Brillouin scattering, stimulated Raman scattering, and electron avalanche breakdown. On the other hand, extrinsic damage includes material flaws or voids, pollutants, and the structure of a material. The laser internal parameters such as spot size of the beam, laser modes, width of the pulse, and laser wavelength also affect the material[38]. Here, the Laser damage threshold was measured through a Q-switched high energy Nd: YAG laser having a wavelength of 1064 nm, pulse Width 10 ns, repetition rate 1-10 pulse per second. As this highly intense laser beam was incident on the 2 mm sample then the energy was absorbed by the material which increased the temperature of the sample. After a particular energy value, there occurs damage/cracks in the material. This energy provides the LDT value for that particular compound. During this experiment, the damage in the crystal was observed through visual formation and the energy value was recorded through the power meter. The power density of the titled compound was calculated by using the formula[35,39]

$$\text{Power density } (P_d) = \frac{E}{\tau A} \quad \ldots (2)$$

where P_d represents the power-density, E signifies the input energy (mJ), τ represents the pulse duration (ns) and A is the spot area (cm^2). The damage threshold value for LHPI comes out to be 1.13 GW cm^{-2} for single shot and 0.78 GW cm^{-2} for 10 shots per second as represented in Table 3. The study revealed that the compound had good laser tolerance thus it may be utilized for device fabrication and other high-power laser-related applications.

3.8 Nonlinear Studies

3.8.1 Second Harmonic Generation

The Non-linear optical characteristic of the LHPI compound was determined by a second harmonic generation experiment. L-histidinium phosphite powder was exposed to a Q-switched high energy Nd: YAG Laser for this purpose. Incoming 1064 nm laser light from the harmonic generator with a 10 Hz repetition rate was used. The second harmonic generation experiment of the sample was carried out by taking KDP as a reference sample. the energy provided to the sample was 0.7 mJ and the output energy coming out of the sample of the titled compound was 5.19 mJ and from the KDP sample was 7.5 mJ as shown in Table 4. The SHG value of L-histidinium phosphite compound was 0.69 times the SHG value for the KDP crystal.

3.8.2 Z-Scan Analysis

For analyzing the third order nonlinearity of material, z-scan method was employed[40]. A crystal with a non-centrosymmetric space group produces second harmonics that may also produce third-order nonlinear effects. The third-order nonlinear effect perturbs the second harmonic wave, causing the pulse to expand. Thus, this effect seems important to understand and must be characterized to generate second harmonics[41]. The Z-Scan method was efficiently used for that purpose. Various nonlinear parameters like nonlinear optical susceptibility, absorption coefficient, nonlinear refractive index (n_2) etc, can be calculated through this method[42]. In this experiment, a highly intense laser pulse of wavelength 800 nm was used for 40 fs. A plano-convex lens with a 40 cm focal length was employed to focus the laser beam on the crystal sample. By focusing the lens, the sample was interpreted from positive to negative regions. The intensity of the output transmittance beam was recorded. The Z-Scan data was drawn to calculate the absorption coefficient (β) and nonlinear refractive index (n_2)

Table 3 — Damage threshold value measured for LHPI sample

Sample	Damage threshold			
	For single pulse/ sec.		For 10 pulse/ sec.	
LHPI	11.3 J cm-2	1.13 GW cm-2	J cm-2	0.78 GW cm-2

Table 4 — SHG measurement for LHPI

Sl. No.	Sample	O/P Energy (mJ)	I/P Energy (mJ)
1	Reference (KDP)	7.5	0.70
2	LHPI	5.19	0.70

as shown in Fig. 12. Initially, for calculating these NLO constants, initially we have to find the effective thickness of the sample which was calculated as[43],

$$L_e = \frac{1-e^{-\alpha L}}{\alpha} \quad \ldots (3)$$

In this relation, α referred to the linear absorption coefficient and L depicted the thickness of the sample. The nonlinear absorption coefficient (β) was evaluated by using the equation[44,45] given below,

$$\beta = \frac{2\sqrt{2}\Delta T}{I_0 L_e} \quad \ldots (4)$$

Here, ΔT was open aperture peak value, I_o was intensity, and L_e was effective thickness. By putting the values of all the parameters, we calculate the value of nonlinear absorption coefficient which come out to be 3.92×10^{-10} cm W^{-1}.

3.9 Shock Damage Threshold

The material damage threshold is a significant statistic that might reflect structural strength. As the soft materials tend to break when pushed under extreme pressure. There are various materials which get negligibly affected from the applied pressure. However, it is a fascinating concern that the material shows the same response under shock loading as it exhibits under static pressure[46]. Non-linear high-pressure phenomenon uses a shock wave as a component which is able to analyze the properties of the material under the influence of different controlled shocks[47]. The action of shock waves on material produces various changes in the material structure. It may result in micro scale distortions, dislocation, lattice orientation defects, twinning of boundary and elastoplastic deformation[48,49]. A high-quality, well-polished single crystal of LHPI was shocked with controlled artificial shock, generated through a semi-automatic pressure-driven shock tube in the laboratory, to ascertain the structural stability of the named compound. In this experiment, a sample crystal was placed against a 1.7 Mach number shock wave, then the studies of surface morphology and powder XRD were analyzed for pre- and post-shock samples.

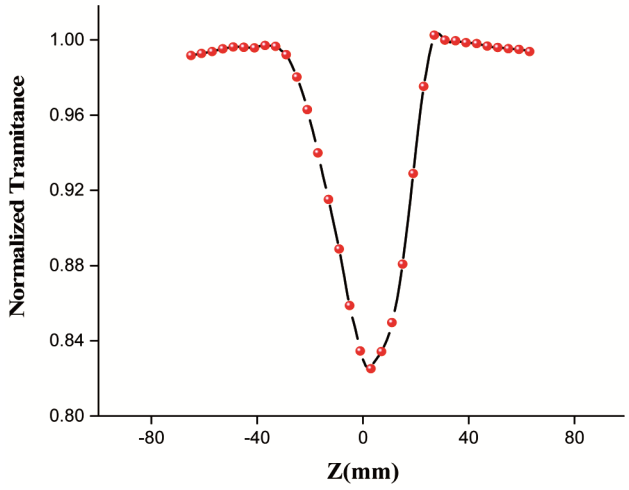

Fig. 12 — Z-scan analysis of LHPI

3.9.1 Surface Morphology

As the sample crystal was exposed to the shock wave produced through the shock tube then there may occur destruction in its surface[50]. This loss might be in the form of any cracks or surface damage to the crystal. For this purpose, a WESWOX optical microscope was used. Control and shock waves (1-5) numbers were used for collecting microscopic photographs of the crystal sample and was given in the Fig. 13. The analysis showed that neither crack nor any damage appears in the crystal after the application of shock wave up to 5 number.

By the application of shock waves, phase-transformation and phase-orientation may occur in the sample[50]. To check these changes in the phase, the sample crystal was analysed under powder XRD with the use of Bruker ASX D2 PHASER for pre- and post-shock load. The diffraction patterns obtained before and after shock application were recorded and analyzed. Figure 14 shows the PXRD pattern of the LHPI compound. The XRD peak matched with that of the monoclinic phase. With increasing the shock load some changes appeared in the XRD pattern. As the 2θ value increases i.e., for $2\theta = 63^0$ and 72^0, peaks with increasing intensity appear with increasing shocks. For S4 a new small peak appears at $2\theta = 82^0$, these new peaks appear due to change in phase orientation.

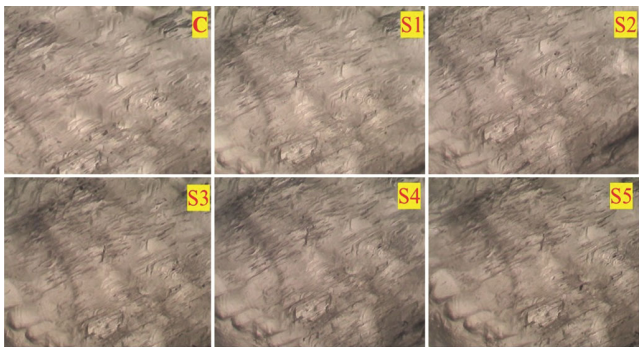

Fig. 13 — Surface morphology under different shocks

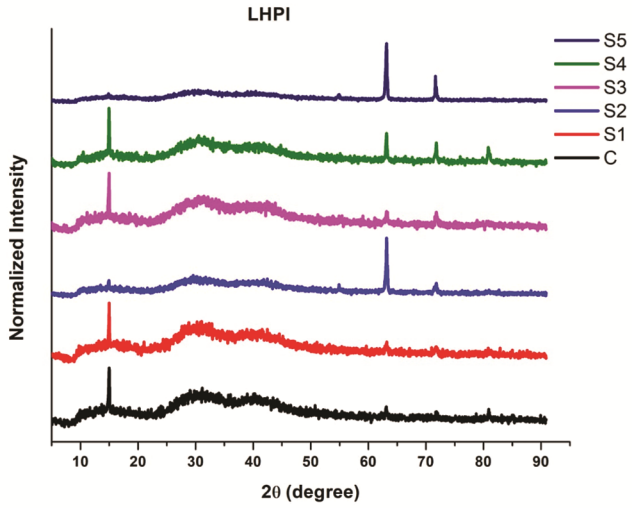

Fig. 14 — PXRD pattern for sample loaded with and without shock waves

3.10 Microhardness Studies

For determining the mechanical behaviour of LHPI crystal, microhardness studies were carried out through Vicker's microhardness test. Under this test, mechanical behaviour was examined through various parameters like- hardness number (H_v), Meyer's index (n)[51]. For this purpose, a well-polished crystal mount on diamond indenter under different loads from 10 gm - 40 gm. Diagonal length and depth value for each load were determined. By using the formula given below Vicker's hardness number was calculated[52].

$$H_v = 1.854 \times \text{applied load (P)}/ (\text{diagonal length})^2 \quad \ldots (5)$$

Here, H_v for hardness number. Using this formula hardness number for each load was calculated and a curve was plotted against the hardness number and applied load. The analysis of the curve explained that the hardness number of the material first increases with load and then decreases similar to LAPI material[53]. For LHPI, H_v Vs Load P curve was represented by Fig. 15. Mayer's Law establishes a relationship between the applied load and the indentation size which was given as[54],

$$P = K_1 d^n \quad \ldots (6)$$

P is the applied load, K_1 is constant, n is Meyer's index and d shows the average length of the diagonal. Meyer's index (n) specifies the behaviour of the material. Onitsch explains the range of n for soft and hard materials. The materials having Meyer's index

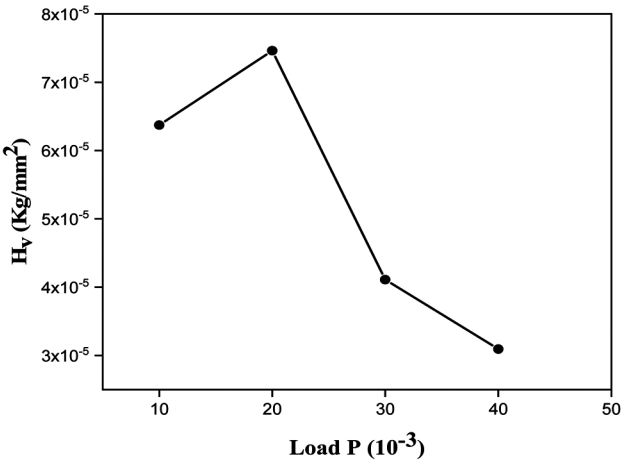

Fig. 15 — H_v Vs Load P plots of LHPI

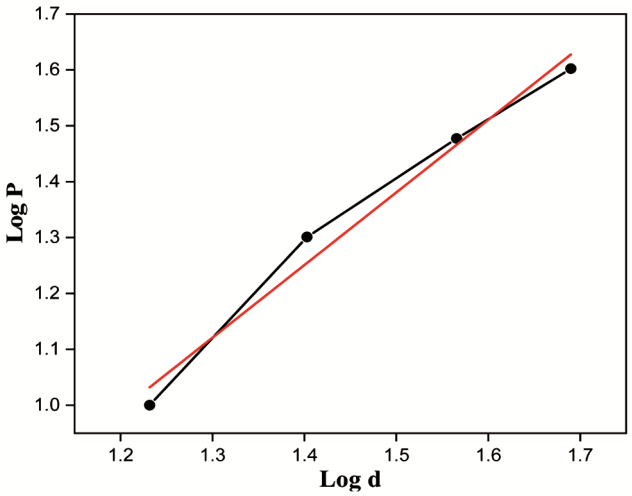

Fig. 16 — Log P Vs Log d curve of LHPI

value between 1 to 1.6 are hard materials but if n is greater than 1.6 then it is soft material[55]. The slope of the curve log P Vs Log d gives the value of n represented in Fig. 16. For the titled compound the value of n comes 1.3 which shows that LHPI is the hard material.

3.11 Polarizability Analysis

Theoretical calculation of polarization of the material was calculated by using the Penn analysis. This analysis can also be measured by Clausius-Mossotti Equation. For calculating the electronic polarizability of LHPI firstly we have to calculate the plasma energy which can be calculated by using the following expression[53].

$$\hbar\omega_p = 28.8\sqrt{\left(\frac{Z\rho}{M}\right)} \quad \ldots (7)$$

Table 5 — Polarizability Parameters of LHPI

Parameters	Values
Plasma Energy	21.86
Penn Energy	8.38
Fermi Energy	18.014
Electric polarizability by Penn Equation	3.91×10^{-23}
Electric polarizability by Clausius- Mossotti Equation	4.0×10^{-23}

In the equation Z stands for the valence electron in the compound, ρ was the density and M was the molecular weight. The Penn energy (E_p) and Fermi energy (E_F) of the material was dependent on the plasma energy and was calculated by using the Eqs. (8) & (9)[56].

$$E_p = \frac{\hbar\omega_p}{\sqrt{(\varepsilon_r - 1)}} \quad \ldots (8)$$

$$E_F = 0.2948(\hbar\omega_p)^{4/3} \quad \ldots (9)$$

Here, ε_r was the dielectric constant at room temperature of LHPI. The electric polarizability was determined by putting the values in the Eq. (10)[53,56].

$$\propto = \left[\frac{(\hbar\omega_p)^2 S_0}{(\hbar\omega_p)^2 S_0 + 3E_p^2}\right] \times \frac{M}{\rho} \times 0.396 \times 10^{-24}\ \text{cm}^3 \quad \ldots (10)$$

In the above formula S_0 was calculated by the relation given below,

$$S_0 = 1 - \left[\frac{E_p}{4E_F}\right] + \frac{1}{3}\left[\frac{E_p}{4E_F}\right] \times \left[\frac{E_p}{4E_F}\right] \quad \ldots (11)$$

Another method to calculate the electronic polarizability is the Clausius- Mossotti equation. The calculated values of the titled compound were given in the Table 5. The Clausius- Mossotti equation was given as[56],

$$\propto = \frac{3M}{4\pi N_A \rho}\left(\frac{(\varepsilon_r - 1)}{(\varepsilon_r + 2)}\right) \quad \ldots (12)$$

4 Conclusion

The transparent NLO active semi-organic L-histidinium phosphite single crystal was successfully grown through SEST. Structural analysis shows that the material crystallizes in monoclinic system with $P2_1$ space group. Sharp peaks of PXRD pattern revealed the good crystalline nature of the material. NMR/ HETCOR peaks are in agreement with the molecular structure. By the photoluminescence study, it was found that the emission spectra of the titled compound correspond to green colour. The Specific heat calculated through the DSC experiment was found to be 13.66 J g^{-1} $°C^{-1}$. The material withstood 1.13 GW cm^{-2} for single shot and 0.78 GW cm^{-2} for 10 shots per second against a highly intense laser of wavelength 1064 nm. LHPI has SHG value 0.69 times the KDP and the non-linear absorption coefficient was calculated to be 3.92×10^{-10} which conclude that LHPI is better material for nonlinear applications. Meyer's index shows that LHPI is a hard material. Thus, the analysis suggests that LHPI is an efficient material for optoelectronics and laser applications. It is best suited for the application needed for second and third harmonic generation material.

References

1 Sun G H, Zhang G H, Wang X Q & Xu D, *J Cryst Growth*, 316 (1) (2011)132.

2 Chen T, Sun Z, Song C, Ge Y, Luo J, Lin W & Hong M, *Cryst Growth Des*, 12 (5) (2012) 2673.

3 Dhanjayan R, Sivakumar N, Gunasekaran S & Srinivasan S, *Mater Lett*, 196 (2017) 74.

4 Liao S M, Du Q S, Meng J Z, Pang Z W & Huang R B, *Chem Cent J*, 7 (1) (2013) 1.

5 Kumari M, Vijayan N, Sharma E, Nayak D, Yadav S, Das S & Pant R P, *J Mater Sci: Mater Electron*, 31 (2020) 18524.

6 Sonia Vijayan N, Vij M, Kumar P, Singh B, Das S & Soumya H *Mater Chem Front*, 1 (6) (2017) 1107.

7 Saminathan P, SenthilKumar M, Shanmugan S, Selvaraju P, Janarthanan B & Sadasivuni K K, *Mater Today Proceed*, 30 (2020) 57.

8 Krishna A, Vijayan N, Verma S, Singh B, Bidkin I, Jayalakshmy M S & Das S, *J Mater Sci Mater Electron*, 28 (2017) 4306.

9 Tyagi N, Yadav H, Hussain A & Kumar B, *J Mol Struct*, 1224 (2021) 129190.

10 Ezhil Vizhi R, Kalainathan S & Baghavan Narayana G, *J Exp Ind Crystallogr*, 42 (11) (2007) 1104.

11 Ghazaryan V V, Zakharov B A, Petrosyan A M & Boldyreva E V, *Acta Crystallogr C: Struct Chem*, 71 (5) (2015) 415.

12 Fleck M, Ghazaryan V V & Petrosyan A M, *J Mol Struct*, 1079 (2015) 460.

13 Madden J J, McGandy E L & Seeman N C, *Acta Crystallogr B: Struct Crystallogr Cryst Chem*, 28 (8) (1972) 2377.

14 Averbuch-Pouchot M T, J *Crystallogr-Cryst Mater*, 207 (1) (1993) 111.

15 Sundari S S, Priya A M, Durairajan A & Valente M A, *J Solid-State Chem*, 300 (2021) 122211.

16 Dolomanov O V, Bourhis L J, Gildea R J, Howard J A K & Puschmann H, *J Appl Cryst*, 42 (2009) 339.

17 Sheldrick G M, *Acta Cryst* A71 (2015) 3.

18 Boffa Ballaran T, Kurnosov A & Trots D, *High Pressure Res*, 33 (3) (2013) 453.

19 Daud A I, Khairul W M, Augustine E, Arshad S & Razak I A, *J Mol Struct*, 1194 (2019) 124.

20 El Bakri Y, Kurbanova M, Ahsin A, Gurbanova F, Ashfaq M, Şahin O & Al-Salahi R, *J Mol Struct*, 1321 (2025) 139896.

21 Babashkina M G, Frontera A, Kertman A V, Saygideger Y, Murugavel S & Safin D A, *J Iran Chem Soc*, 19 (1) (2022) 85.

22 Essid M, Muhammad S, Marouani H, Saeed A, Aloui Z & Al-Sehemi A G, *J Mol Struct*, 1211 (2020) 128075.

23 Ashfaq M, Tahir M N, Muhammad S, Munawar K S, Ali A, Bogdanov G & Alarfaji S S, *ACS omega*, 6 (46) (2021) 31211.

24 Ashfaq M, Khalid M, Tahir M N, Ali A, Arshad M N & Asiri A M, *ACS omega*, 7 (11) (2022) 9867.

25 Seth S K, *Acta Crystallogr E: Crystallogr Comm*, 74 (5) (2018) 600.

26 Spackman P R, Turner M J, McKinnon J J, Wolff S K, Grimwood D J, Jayatilaka D & Spackman M A, *J Appl Crystallogr*, 54 (3) (2021) 1006.

27 Sert Y, Gümüş M, Gökce H, Kani İ & Koca İ, *J Mol Struct*, 1171(2018) 850.

28 Ravisankar V, Ramesh V, Gunasekaran B, Krishnamohan M, Girisun T S & Dhanusha A, *ECS J Solid-State Sci Technol*, 10 (9) (2021) 091008.

29 Chandran S, Paulraj R & Ramasamy P, *Optic Mater*, 73 (2017) 154.

30 Chandran S K, Paulraj R & Ramasamy P, *Spectrochim Acta A: Mol Biomol Spectrosc*, 151 (2015) 432.

31 Anitha M, Ravindran B & Vijayalakshmi M, *Mater Today: Proceed*, 45 (2021) 8162.

32 Suresh T, Vetrivel S, Gopinath S & Vinoth E, *J Mater Sci: Mater Electron*, 31 (2020) 13310.

33 Hasmuddin M, Abdullah M M, Singh P, Shkir M, Vijayan N & Wahab M A, *Optic Laser Technol*, 74 (2015) 53.

34 Murugesan M, Paulraj R, Perumalsamy R & Kumar M K, *Appl Phys A*, 126 (2020) 1.

35 Peramaiyan G, Pandi P, Sornamurthy B M, Bhagavannarayana G & Kumar R M, *Spectrochim Acta A: Mol Biomol Spectrosc*, 95 (2012) 310.

36 Muthuraja A & Kalainathan S, *Mater Res Innov*, 21 (1) (2017) 50.

37 Ghandiparsi S, Chatterjee B, Shen J X, Gottlieb M S, Frye C D, Schneider J D & Voss L F, *Adv Mater Interfaces*, 12 (2) (2025) 2400639.

38 Boling N L, Crisp M D & Dube G, *Appl Optic*, 12 (4) (1973) 650.

39 Justin P, Anitha K, Ahamed M B & Vijayaraghavan G V, *J Mater Sci: Mater Electron*, 30 (2019) 9735.

40 Dhatchaiyini M K, Rajasekar G & Bhaskaran A, *J Mater Sci*, 54 (13) (2019) 9362.

41 Aswaniya K, Raj M J, Gowri S & Vinitha G, *J Mol Struct*, 1218 (2020) 128460.

42 Kumar K, Rajathi S, Vincent V C, Sangeetha R, Bakiyaraj G, Manivannan D & Vinitha G, *Optik*, 247 (2021) 167880.

43 Vij M, Yadav H, Vashistha N, Kumar P & Maurya K K, *J Mol Struct*, 1206 (2020) 127759.

44 Bhuvanesawri R, Bharathi M D & Murugesan K S, In *IOP Conf Series: Mater Sci Eng,* 360 (1) (2018) 012059.

45 Anis M, Hakeem D A & Muley G G, *Result Phys*, 6 (2016) 645.

46 Song Y, Yu G, Jiang L, Zheng X, Liu Y & Yang Y, *J Appl Phys*, 109 (7) (2011) 073103.

47 Sivakumar A, Dhas S S J & Dhas S M B, *Solid State Sci*, 110 (2020) 106452.

48 Larson D B, *J Appl Phys*, 38 (4) (1967) 1541.

49 Kuksin A Y, Stegaĭlov V V & Yanilkin A V, *Dokl Phys* 53 (2008) 287.

50 Jagadeesh G, *Resonance*, 13 (2008) 752.

51 Mohamed M P, Sudha S, Jayaprakash P, Vinitha G, Nageshwari M, Sangeetha P & Caroline M L, *Chin J Phys*, 60 (2019) 581.

52 Robert R, Raj C J, Krishnan S, Uthrakumar R, Dinakaran S & Das S J, *Phys B: Condens Matter*, 405 (16) (2010) 3248.

53 Sonia Vijayan N, Vij M, Krishna A, Yadav H, Maurya K K & Kumar P, *Appl Phys A*, 125 (2019) 1.

54 Rajyalakshmi S, Rao K R, Brahmaji B, Samatha K, Rao T V & Bhagavannarayana G, *Optic Mater*, 54 (2016) 74.

55 Jothi R A, Vetrivel S, Gopinath S, Mullai R U & Vinoth E, *Appl Phys A*, 127 (7) (2021) 496.

56 Rathee S P, Ahlawat D S, Dhas S M B, Maurya K K, Singh B & Bdikin I, *Mater Sci Eng: B*, 264 (2021) 114927.